Ochoa Nelio A. (Orcid ID: 0000-0001-8799-5132)

pH RESPONSIVE GUM TRAGACANTH HYDROGELS FOR HIGH METHYLENE BLUE ADSORPTION

Cristian O. Illanes, Eduardo A. Takara, Martin A. Masuelli, and Nelio A. Ochoa *

Instituto de Física Aplicada (INFAP), Departamento de Química, Facultad de Química, Bioquímica y Farmacia, Universidad Nacional de San Luis, CONICET, Ejército de los Andes 950, D5700HHW, San Luis, Argentina.

ABSTRACT

Background

Biobased hydrogels are used in many applications due to their easy availability, low cost and versatility to acquire different structures. However, there is scarce information about the changes generated in the matrix's microstructure after crosslinking reactions. The effect of the crosslinking reaction using glutaraldehyde on the micro and macrostructure of tragacanth gum hydrogels (TG GLU) was evaluated.

Results

New acetal groups, that increase with increasing GLU, produced less packed biopolymeric structures with more thermal stability. Due to demethoxylation, a higher amount of free carboxylic groups after crosslinking reaction were determined in TG GLU. Crosslinked hydrogels presented a higher water uptake capacity with a pH responsive behavior with suitable thermal and mechanical properties. Besides, the highest adsorptive capacity of methylene blue achieved was q_m=530 mg/g.

Conclusions

pH responsible gels from tragacanth were obtained after crosslinking with glutaraldehyde. Chemical and microstructural changes affect the Methylene Blue adsorption, resulting in hydrogels with improved adsorptive properties. These properties give the TG-GLU hydrogels some features that make them suitable for practical applications related to the pharmaceutical industry for drug delivery and water remediation.

*Corresponding Author
Dr. Nelio Ariel Ochoa
E-mail: arielochoaunsl@gmail.com

Keywords: Tragacanth gum - Crosslinking - pH responsive hydrogels - Methylene blue adsorption

This article has been accepted for publication and undergone full peer review but has not been through the copyediting, typesetting, pagination and proofreading process which may lead to differences between this version and the Version of Record. Please cite this article as doi: 10.1002/jctb.7507

1. Introduction

Natural gums are used in a wide range of applications due to their easy availability, low cost and versatility to acquire different structures [1–5]. TG is a complex heterogeneous anionic polysaccharide obtained from herbs and shrubs of Asian *Astragalus* species such as *A. gummifer, A. gossypinus* and *A. microcephalus* [6]. Several researchers have studied the chemical structure of TG. However, the complex structure has not yet been entirely elucidated [7,8]. Two fractions have been described: tragacanthine which is water soluble and is composed of tragacanthic acid and a small amount of arabinogalactan, and bassorine, which is insoluble in water. Bassorine is a lineal polymer of arabinogalactan containing D-fucose, D-xylose, L-arabinose, D-galactose and D-galacturonic acid methyl ester [6,9]. Furthermore, significant similarities in the structure of bassorine and ramnogalacturonano I (RG-I) of pectin have been reported in literature [10,11].

Carboxylate groups are responsible of the strong hygroscopic properties of TG [12]. However, such a hydrophilic matrix causes a high-water solvation of biopolymer chains that not allow its use as a gel. This issue can be solved by crosslinking with glutaraldehyde (GLU) [12–14]. The reaction time and the crosslinker concentration are the main variables that influence the properties of hydrogels, such as hydration and mechanical resistance [15]. Kiani *et al.* prepared TG hydrogels using glycerol, ethylene glycol, and triethylene glycol as plasticizers and GLU as crosslinker [8]. These authors determined a greater swelling capacity as GLU concentration increases. In addition, they reported the dependence of the swelling values on the percentage of carboxylate groups. Rahimdokht *et al.* prepared TG–GLU hydrogels with TiO_2 nanoparticles as photocatalysts for methylene blue degradation [16]. A consolidated gel structure was observed, whereas a high dye degradation was determined in all photocatalysts. Such behavior was attributed to the high attractive force established between the negatively charged nanoparticles, the carboxylate groups of the TG and the positive charge of the dye.

The crosslinking degree influenced the thermal properties of carboxymethyled TG crosslinked with GLU (CMTG-GLU) [12]. At T=500 ºC, a 55 % weight loss was observed on the CMTG-GLU curve, compared to 62 % and 65 % for CMTG and TG, respectively. In addition, the adsorption of water in the matrix was also influenced by crosslinking, the highest free swelling capacity and centrifuge retention capacity of CMTG-GLU was observed at pH 8 for a ratio of 20 % by weight of GLU to CMTG.

Self-repairing TG hydrogels prepared with GLU and citric acid (TG-GLU and TG-CA, respectively) can withstand multiple cycles of polymerization and rupture while

maintaining their mechanical properties [17]. Methylene blue is a molecule with reported pharmacological [18] and potential medical [19] applications and is mainly used as a dye. However, it has high toxicity, so its removal from water is frequently reported in different sorbents [20–25]. Therefore, this cationic dye is a test molecule to evaluate the adsorption capacity of different anionic hydrogels.

Nowadays, there is scarce information about the changes generated in the TG matrix's microstructure after crosslinking with GLU and their impact on the whole hydrogel properties. Therefore, this work aims to study changes generated in the micro and macrostructure of pH-sensitive hydrogels of TG crosslinked with GLU. The hydrogel matrices were investigated by infrared spectroscopy (FTIR), X-ray diffractometry (XRD), thermal analysis, and scanning electron microscopy (SEM). In addition, functional hydrogels properties such as solubility assays (S), swelling index (Sw), ionic exchange capacity, mechanical behavior and methylene blue adsorption were determined.

2. Materials and Methods

2.1. Materials

A commercial TG powder (CAS Number 9000-65-1) with an average MW=840 kDa determined by viscosimetric measurements [26] was supplied by Sigma-Aldrich. Glutaraldehyde (GLU, grade II 25 %), hydrochloric acid (HCl, 37%), glycerol, acetone, ethanol, *N,N*-dimethylformamide (DMF), and chloroform of analytical grade were purchased from Sigma-Aldrich (Argentina). The chemicals were used as received without further purification and all solutions were prepared with ultra-pure water (resistivity > 1.8 mΩ).

2.2. TG Hydrogels preparation

TG hydrogels were prepared by dissolution of tragacanth gum 2 % w/v in 50 mL of water, and then glycerol was added gradually (0.5 % w/v) under stirring for 2 h at 40 °C. This plasticizer is required to avoid extensive intermolecular forces that produce brittle hydrogels [27]. The TG solutions were placed on Petri dishes (14.5 cm internal diameter) and dried at 60 °C for 24 h. After, the TG samples were crosslinked by immersion in a solution containing 50 mL of acetone, glutaraldehyde and HCl 1 % w/v.

The contact time and GLU concentration were varied between 0 to 48 h and 0 to 10 % w/v, respectively. Finally, the hydrogels were washed with deionized water until neutrality. The preparations were carried out in triplicate.

Hydrogels crosslinked during 24 h were individualized as TG GLU-5, TG GLU-7, and TG GLU-10 for GLU concentrations of 5, 7, and 10, respectively. Samples used in the reaction kinetic study were identified as TG GLU - x - 12, TG GLU - x - 24 and TG GLU - x – 48 (where x = 5, 7 or 10).

2.3. Hydrogels characterization

2.3.1. Infrared spectroscopy

FTIR spectra were determined with a Varian 640 Spectrometer using ATR mode. The samples were dried at 60 °C for 48 h before performing the measurements. Spectra were recorded after 64 scans with a resolution of measurement range between 4000 and 500 cm^{-1} at ambient temperature.

2.3.2. X-ray diffractometry

The structures of the hydrogels were characterized with a Rigaku model D-Max III C X-ray diffractometer with an angular range from θ = 5° to 60°. The equipment was operated at 30 kV (λ = 0.15418 nm) with a Cu Kα lamp and nickel filter. The relative intensity was taken at room temperature with a step size of 0.02. The samples were cut into rectangles and dried at 60 °C for 48 h. The d-spacing (d_{sp}) of each film was determined using Bragg's equation (Eq. (1)).

$$n\lambda = 2d\ sin\ \theta \qquad \text{(Eq. 1)}$$

2.3.3. Thermal analysis

Thermal properties of neat TG and TG GLU were determined by a TA analyzer model SDT-Q600 (TA instruments, Lindon, UT, USA) recording simultaneously thermogravimetric data (TGA) coupled with derivative thermogravimetry (DTG). A first scan was performed from 25 to 105 °C to dry the samples. After cooling, a second scan

was performed over the range of temperature from 25 to 500 °C with a heating rate of 10 °C min^{-1} under N_2 atmosphere (flow rate of 50 mL min^{-1}).

Differential scanning calorimetry (DSC) measurements were recorded on a MDSC 2920 TA instrument, Inc., New Castle, USA. The operating conditions were as follows: (a) heating rate: 10 °C min^{-1}, (b) atmosphere: N_2 (99.99 %) at a flow rate of 50 mL min^{-1}, and (c) weight sample: 10 mg. DSC temperature axes were calibrated with indium (99.99 %, mp 156.60 °C). Empty aluminum pans (40 mL) were used as references. Reported data were processed with the Thermal Solutions® software (TA Instrument, Inc.). At least three specimens of each sample were recorded, and the average of thermograms was collected. The same scans of temperature used in TGA were performed in this analysis.

2.3.4. Scanning electronic microscopy

The surface morphology and the hydrogels cross section were studied using a LEO 1450VP microscope. All samples were previously lyophilized in a chamber of a freeze-drier (Labconco 7740030; Labconco Corp., Kansas City, MO, USA), operating at −45 °C and 0.05 mbar for 12 h. After that, the hydrogels were fractured in liquid nitrogen and covered with gold. All measurements were performed with an accelerating voltage of 10 kV with a secondary electron image as a detector.

2.4. Hydrogels properties

2.4.1. Solubility assays

The solubility of the hydrogels in different solvents was investigated. Assays were carried out by immersing the matrices into water (at 25 and 50 ºC), acetone, ethanol, DMF and chloroform for 120 h at 25 ºC. The loss of mass was determined by weighting before and after solvent contact.

2.4.2. Swelling index

The swelling index **(S_w)** was determined to indicate pH sensitivity. The S_w studies were performed by cutting circles (1 cm diameter) of the hydrogels, which were dried at 60 °C until constant weight (W_d). After that, the hydrogels were immersed in 5 mL HCl

or NaOH aqueous solutions at different pH values (3, 7 and 11) at room temperature for 24 h. Buffer solutions are not suitable for pH adjustment since the ions in the buffer solutions affect the ionic strength of hydrogels. Tissue paper was used to remove the excess of water on the hydrogel surfaces and then samples were weighed (W_s). Swelling index was calculated by equation 2.

$$\mathbf{S_w} = \left(\frac{W_s - W_d}{W_d}\right) * 100 \qquad \text{(Eq. 2)}$$

where, W_d and W_s correspond to the weights of the dry and swollen hydrogels, respectively. All measurements were performed by triplicate and standard deviations were calculated.

2.4.3. Ionic exchange capacity

Samples were contacted with a 0.1 M HCl for 12 h. Next, acidic hydrogels were washed several times with distilled water and immersed into a 1.0 M NaCl aqueous solution. Subsequently, the hydrogels were removed and the remaining solutions were titrated with a 0.01 M NaOH aqueous solution to determine the concentration of exchanged protons. Ionic exchange capacity (IEC) is expressed as meq H^+ g^{-1} of dry hydrogels.

2.4.4. Mechanical properties

Tensile tests of the prepared TG and TG GLU hydrogels were performed at room temperature using a CT3 Brookfield texturometer according to ASTMD882 [28,29]. Hydrogel samples were stored in a humidity and temperature-controlled chamber for 24 h at 25 °C and 75% relative humidity to ensure the complete relaxation of the polymeric structures and standardize the experimental procedure. Under these conditions, the tensile strength was determined at a constant traction speed of 5 mm min^{-1}. The recorded data of three hydrogel samples were averaged and the standard deviation was calculated. The film thickness was measured using a Köfer micrometer (precision ± 1 µm, Germany).

2.4.5. Methylene blue adsorption studies

Batch adsorption studies of aqueous methylene blue (MB) solutions (20 mL) were performed in a test tube containing 0.1 g of dried hydrogels with constant agitation (150 rpm) at 25°C for 24 hours. MB concentrations ranged from 10 mg/L to 250 mg/L and

HCl or NaOH solutions were added to maintain pH values of 3 or 11. After equilibrium, MB concentrations were determined with an UV/visible spectrophotometer (Hitachi UV-2001) at λ=663 nm using calibration curves determined at pH assayed due to changes in absorptivity molar coefficients. Langmuir isotherm was used to fit the experimental data by the following equation:

$$q_e = \frac{q_m b C_e}{1 + b C_e} \quad \text{(Eq. 3)}$$

where C_e is the concentration of adsorbate at equilibrium (mg/L), q_e and q_m are equilibrium and maximum adsorption capacity of adsorbent (mg/g), respectively and *b* (L/mg) is the Langmuir constant.

2.4.5.1. Thermodynamic and kinetics study

To study the MB adsorption on TG GLU, kinetic and thermodynamic parameters were determined. MB adsorption experiment was performed at various temperatures (15, 25 and 35 °C) and the process kinetics was observed using UV-Vis spectrometry measurements before equilibrium was reached. The thermodynamics parameters were calculated using the below equations (Sheela and Nayaka, 2012).

$$K_c = \frac{q_e}{C_e} \quad \text{(Eq. 4)}$$

$$\Delta G^{\circ} = -RT ln K_c \quad \text{(Eq. 5)}$$

$$ln K_C = \frac{\Delta S^{\circ}}{R} - \frac{\Delta H^{\circ}}{RT} \quad \text{(Eq. 6)}$$

The linear plot of In Kc with 1/T gives the values of ΔH^{o} from slope and ΔS^{o} from intercept.

To study the adsorption kinetics pseudo-first-order and pseudo-second-order models were used (See, SM 7: kinetic models).

3. Results and discussion

3.1. Hydrogels characterization

In figure 1A, it can be seen the FTIR bands of TG without crosslinking. The main band zones can be addressed as: -OH at 3100-3500 cm^{-1} region, bands at 2931–2856 cm^{-1} were attributed to -CH, -CH_2, and -CH_3 groups in pyranose ring, glycerol, and methoxyl residues on carboxylic acid groups. Besides, bands between 1749-1620 cm^{-1} were assigned to carbonyl groups in TG as in methoxyl residues and free carboxylic groups (protonated and deprotonated). In the range from 1450 to 1250 cm^{-1} are found the bands corresponding to C-OH bending, -C-O-CH_3 asymmetric and symmetric stretching and O-C-O symmetric stretching. The stretching band of C-C of the pyranosic ring and C-O groups of glycosidic bonds can be observed below 1200 until 1025 cm^{-1}. This spectrum was similar to that reported by other researchers [30].

GLU concentration and reaction time were varied to analyze changes in the bands of crosslinked TG. As shown in the supplementary material (SM 1), after 12 h of reaction time, the spectra of crosslinked samples have no changes indicating that the reaction did not proceed. In figure 1A) and 1B), the spectra of neat TG and crosslinked samples at different concentrations are shown. As the concentration of GLU increases, the -OH band diminishes in intensity and widens (Fig. 1A). This behavior was expected since GLU reacts with the -OH groups forming acetal bonds and thus decreasing the density of hydrogen bonds in the structure of TG [31].

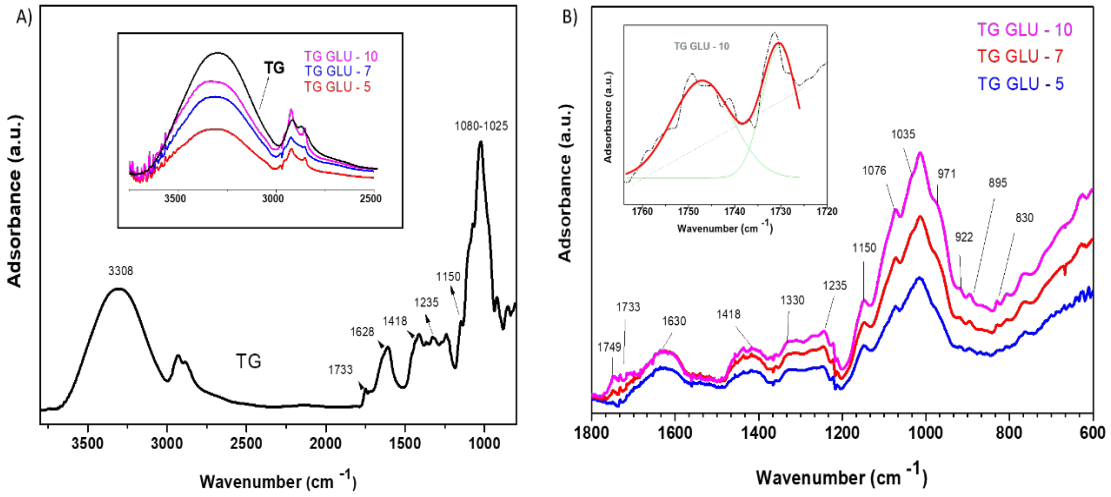

Figure 1: spectrum FTIR A) TG and -OH bands of TG GLU B) 1800 - 600 cm^{-1} range of TG GLU spectra and deconvolution of the region 1750 - 1733 cm^{-1} for TG GLU-10.

Carboxylate anion gives rise to a strong absorption band at 1620 cm^{-1}. Between 1700 cm^{-1} and 1750 cm^{-1} a band with two shoulders appears. According to Silverstein *et al.*, aliphatic esters have a major force constant in carbonyl groups compared to

protonated carboxylic acids [32]. So, the band shoulders indicate two different carbonyl groups in that spectrum region (fig. 1B). We applied the method reported by Fellah *et al.* to determine the degree of methyl esterification in TG using the band at 1010 cm^{-1} corresponding to the skeletal backbone as reference [33]. Also, deconvolution of the mentioned band was performed with the Origin Software (deconvolutions of TG GLU-5 and TG GLU- 7, see SM 2). The band ratio 1450/1010 diminishes as GLU concentration increases, indicating that the methoxylation degree is lower for crosslinked TG GLU samples. TG band ratio 1450/1010 was 1.23, while values of 0.76, 0.51 and 0.49 were determined for TG GLU-5, TG GLU-7 and TG GLU-10, respectively. Simultaneously, free carboxylic acid groups increase as Glu concentration rises. The TG band ratio of 1735/1010 was 0.11, while values of 0.13, 0.17 and 0.25 were calculated for TG GLU - 5, TG GLU - 7 and TG GLU -10, respectively. In addition, IEC of TG GLU - 5, TG GLU - 7 and TG GLU - 10 samples was determined, resulting in values of 0.18, 0.36 and 0.58 meq g^{-1}, respectively. This upward trend in IEC follows the rise of free carboxylic groups content in TG GLU. Such behavior was unexpected during TG crosslinking. Usually, GLU reacts with –OH to give acetals by forming ion acyliums intermediate due to acid media of reaction. However, commercial GLU used in this study was an aqueous solution (25 % wt.). Thus, when GLU concentration increases, the water concentration in the reaction media also increases. The H_3O^+ ions can generate the protonation of alkyl-oxygen of the ester given an acylium ion (from ester carbonyl) intermediate, which is unstable due to water or alcohol molecules are good leaving groups [34]. As a result, free carboxylic acid groups were generated by ester hydrolysis. This reaction occurs simultaneously with TG crosslinking.

In Figure 2, diffractograms of TG and crosslinked TG are shown. TG accommodates in a broad amorphous phase centered at $2\theta = 21.8°$, which corresponds to d_{sp} of 4.08 A°. A similar spectrum with a wider band located at $2\theta = 26.7°$ has been reported [35,36].

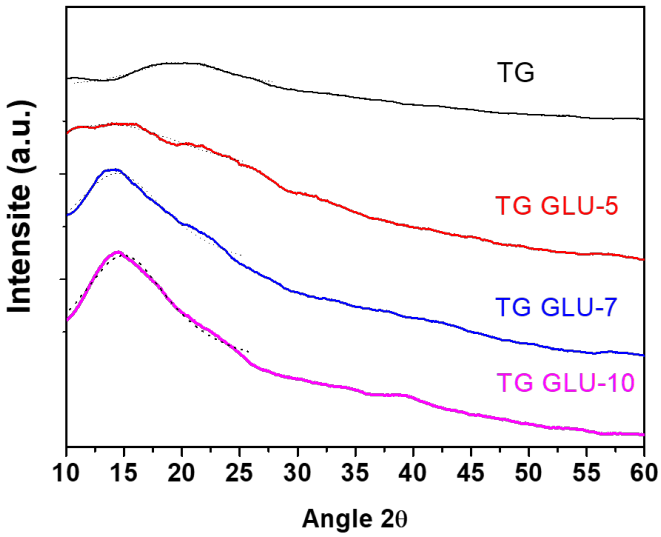

Figure 2: XRD spectra of TG and crosslinked TG.

After crosslinking, the bands of TG GLU samples were more intense and a shift to lower angle values was observed. d_{sp} values of 5.91, 6.14 and 6.51 were determined for TG GLU - 5, TG GLU - 7 and TG GLU - 10, respectively. TG was the least ordered packed structure, but more organized structures were obtained after crosslinking. Similar results were reported by Mohammadian et al. when crosslinked gum tragacanth/poly (vinyl alcohol)/Ag^{o} with GLU [37].

New covalent bonds generated by GLU in the matrix of TG diminish the -OH groups. The higher intensity of the band in the TG GLU samples can be attributed to the number of ester and free carboxylic groups, which affect the solvation and packing of neat and crosslinked TG samples. Ester groups are hydrogen bond acceptors, whereas free carboxylic groups can act as either hydrogen donors or acceptors. As a result, the hydration shell surrounding –COOH groups is greater than that corresponding to the ester groups [38]. These phenomena generate an increase in the packaging of the polymeric matrix of the neat hydrogel.

Thermogravimetric analysis of DTG and DSC was performed to characterize neat and crosslinked TG samples, as shown in figure 3. The TGA obtained can be observed in SM 4.

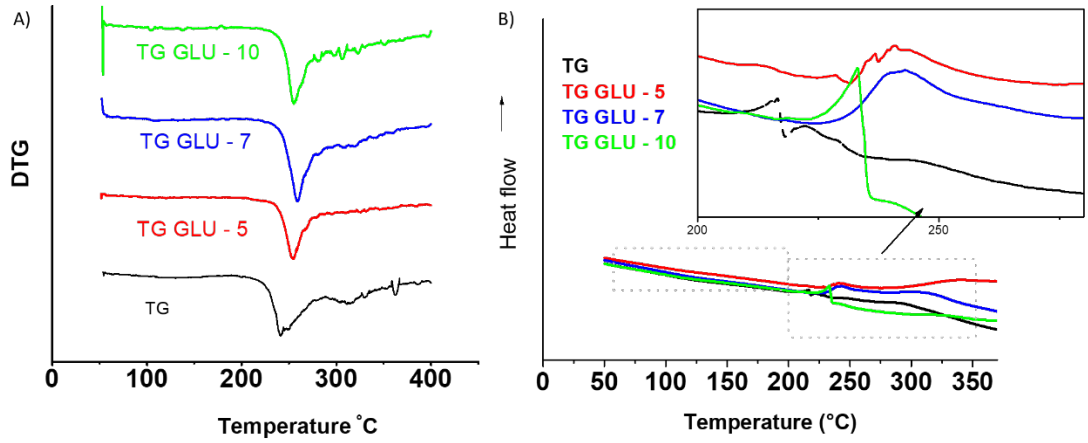

Figure 3: Thermogravimetric analysis of neat and crosslinked TG samples A) DTG and B) DSC.

TGA showed a first stage weight loss of 4.3 % with an inflection point at 153 °C due to dehydration. Physically adsorbed water and water molecules linked to weak hydrogen bonds are responsible for this dehydration process. The second stage of weight loss of 36 % started at 235 ºC with a maximal weight loss rate at 246 ºC. In this temperature range, the thermal decomposition of TG begins, finalizing with a decomposition stage at 350 ºC. Similar results were reported [39–41].

Recently, pectin degradation studies revealed a complex process that includes demethoxylation, depolymerization by backbone hydrolysis and cleavage of neutral sugar side chains [42,43]. Such processes require water molecules and therefore are affected by moisture content. Other depolymerization processes observed in pectins were β-elimination and decarboxylation, which do not require water. However, it was determined that decarboxylation of D-galacturonic acid residues occurred between 191-295 °C. Above this temperature, there was no release of CO_2. This process can take place in TG degradation as well. Thus, the two-stage decomposition pattern can be explained due to the occurrence of such depolymerization processes. It is well known that crosslinking increases the thermal stability of biopolymers [44,45]. The loss of -OH groups due to crosslinking reaction, the formation of new acetal bonds and the increase of hydrogen bonds with carboxylic acid groups favor the strong interactions between TG chains. As a result, higher thermal stability was observed in crosslinked TG samples. The maximal weight loss rate at 265 °C, 270 °C and 278 °C were determined for TG GLU - 5, TG GLU - 7 and TG GLU -10, respectively. More details about thermogravimetric events of all TG hydrogels can be seen in Table SM 1.

As shown in figure 3B), after the endothermic hydration process, TG showed an endothermic pre-peak at 217 °C before exothermic degradation peak in DSC measurements. Similar pre-peaks have been observed in pectin by Pasini Cabello *et al.*[46] and Einhorn-Stoll [47] related to a conformational change of galacturonan ring. After crosslinking, no pre-peak was observed. However, exothermic peaks due to degradation shift to higher temperatures than neat TG.

In figure 4, SEM images show no significant topography changes in TG GLU. TG and TG GLU -5 are also presented for comparison. Surface micrographs of TG and TG GLU -5 show an interconnected nodular topography for both samples (Fig. 4A and 4B). In figure 4C and 4D, the cross-section of TG and TG GLU -5 samples can be seen.

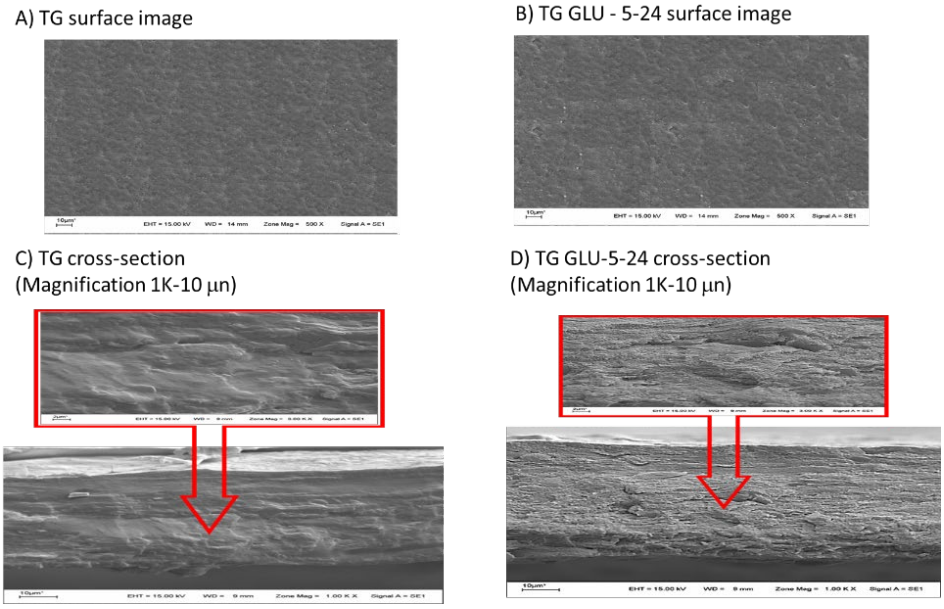

Figure 4: surface and cross-section of TG and TG GLU -5.

TG has a dense and compact morphology, whereas TG GLU-5 presents a layered structure. This result can be explained by the loss of -OH groups and the formation of free carboxylic groups simultaneously. Such changes in the balance between intra- and intermolecular hydrogen bonds can disrupt highly packed zones losing the dense morphology of neat TG.

3.2. Hydrogels properties

The solubility of the hydrogels in different solvents was also investigated, showing that TG GLU were insoluble in the different solvents studied (table SM 2). To

understand the effect of the crosslinking on the gel properties, one of the most common approaches is to determine the swelling capacity [48,49]. The water absorption is due to the presence of hydrophilic groups such as –OH, –COOH, among others. The swelling index of TG GLU samples was determined as it was described in the experimental section. In Figure 5A), the correlation between $\mathbf{S_w}$ vs. d_{sp} was obtained to corroborate the effect of hydrodynamic free volume on water uptake. Also, the correlation between $\mathbf{S_w}$ vs. -COOH groups obtained by a band ratio of 1735/1010 is shown in Figure 5B). Ionic interactions between chains of the gums cause swelling, which depends on the GLU concentration during the network formation [50]. After crosslinking, the increase in hydrophilic -COOH groups increases the free volume of the chains. Higher free volume can be due to both the ionic repulsion and greater hydration shell of the new carboxylate groups. As a result, the increased hydrophilic character of crosslinked hydrogels facilitates water absorption.

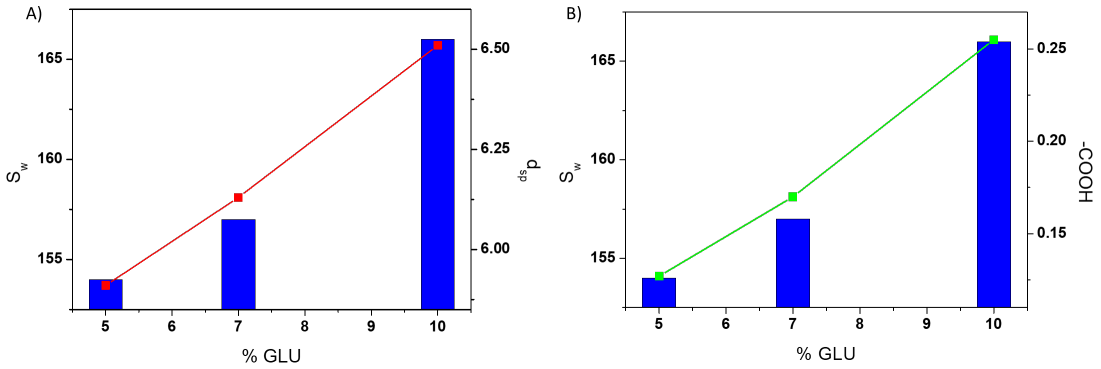

Figure 5: Swelling index (bar graph) of TG GLU vs. (A) d_{sp} (line graph) and (B) band ratio of -COOH (line graph).

Figure 6 shows the impact of pH on $\mathbf{S_w}$ for TG-GLU samples. A higher amount of water molecules adsorbed was obtained as pH values increased. This property of crosslinked hydrogels was addressed to their pH responsible behavior. The rise in swelling with crosslinking (at the same pH) is consequent with the enhanced hydrophilicity of the crosslinked matrix due to the increase in the carboxyl functionality within the matrix. In a pH range between 3.0 and 11 (for the same hydrogels), the $\mathbf{S_w}$ increases with the increase in pH. At a lower pH, the chains are protonated and tightly packed by hydrogen bonding. However, as the pH increases, the carboxylic acid groups are ionized and the repulsion forces between the carboxylate anions are raised, allowing

a higher hydration shell to enhance the S_w. Singh and Sharma also observed significant changes in the swelling pattern of TG [51].

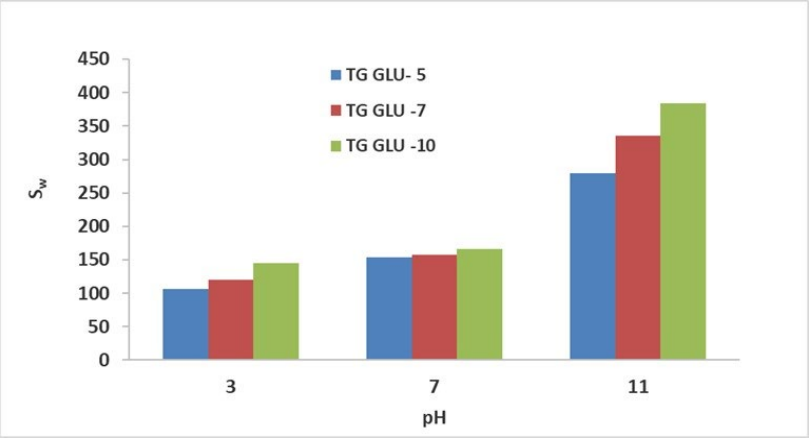

Figure 6: pH responsive behavior of TG-GLU hydrogel.

The most extensive parameters that describe mechanical properties are tension at break (TS), elongation at break (% E) and Young's modulus (Me). Tension at break is the maximum stress a material can withstand before rupture [52]. Elongation at break is the percent elongation of the film concerning its initial length and is a measure of material stretching capability. Young modulus, or elastic modulus, indicates the film's rigidity [53,54]. Hydrogel mechanical measurement results are presented in figure 7. Crosslinked samples had higher TS values because new covalent bonds were formed. However, the more unpacked structure of neat TG shows slightly less elongation than crosslinked TG. This fact corroborates that the TG-GLU structures had stronger intermolecular interactions, which might be due to simultaneous crosslinking and demethoxylation reactions.

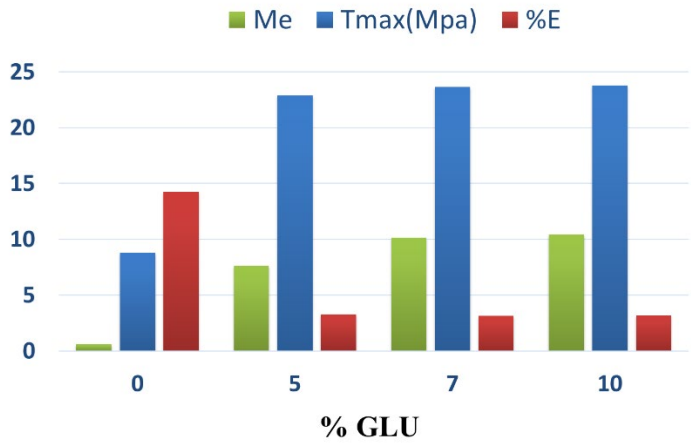

Figure 7: Mechanical properties TG GLU.

Increasing carboxylic groups on the gel structure affect its Methylene Blue adsorption capacity. In SM 6, the adsorption isotherms can be seen in Figure SM 5 and Table SM 3 the values of maximum adsorption capacity (q_m) and Langmuir adsorption constant (b) for each isotherm are reported. An increase of q_m in all the prepared hydrogel can be seen after the carboxylate groups are deprotonated at pH =11. Therefore, such maximum adsorption capacity increases following the increase of carboxylate groups in the hydrogel, i.e. q_m increases for TG10>TG7>TG5. Both trends confirm that due to the rise of deprotonated carboxylic groups, the cationic pigment was adsorbed to a greater extent on the more negatively charged hydrogel. However, the Langmuir b parameter decreases for those hydrogels prepared using higher GLU concentrations. Figure 8 shows a decrease in b values as the d-spacing values increase. This trend indicates that the larger hydrogel hydration cell affects the binding energy between MB and the adsorption sites.

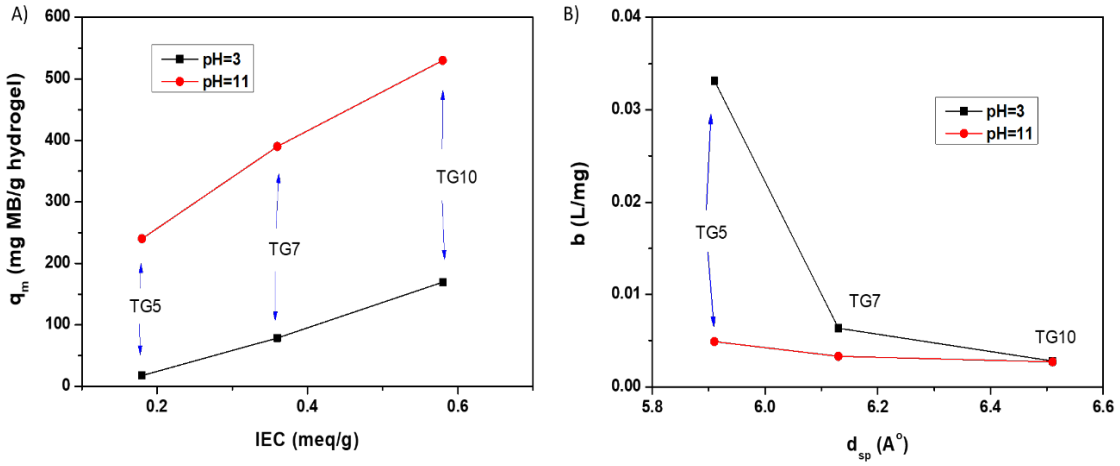

Figure 8: Langmuir parameters analysis at 25 °C. A) b at different pH as a function of d_{sp}. B) q_m at different pH as a function of IEC.

Table SM 4 provides the thermodynamic parameters of sorption MB onto TG GLU hydrogels. The ΔH^o values exhibited by TG GLU hydrogels at pH 11 indicates that the sorption process was endothermic. The low positive ΔS values demonstrate the increased randomness at the solid-solute interface and the affinity of TG GLU hydrogels for the MB (Aroguz et al., 2008). However, the negative values of ΔG^o reveal a spontaneous physisorption process based in enthalpic effects. The sorption process of MB on TG GLU hydrogels at pH 3 presented similar thermodynamic behavior. However,

adsorption enthalpies of TG GLU hydrogels at pH 11 were higher than pH 3, so more energy was necessary to supply to adsorb MB onto TG GLU hydrogels at pH 11.

The kinetic pseudo second order model presents the higher linear correlation coefficients, R^2 greater than 0.99 in all cases (see, SM 5). As general trend, it can be observed that kinetic constants obtained at pH 3 in TG GLU hydrogels are higher than pH 11. These results can be correlated to the behavior observed considering the b Langmuir constant mentioned before. As b Langmuir constant increases, kinetic constant increases as well.

The TG hydrogels investigated have demonstrated a notably enhanced MB adsorption capacity compared to alternative adsorbents as it has been reported in literature (table SM 6).

CONCLUSIONS

pH responsible gels from tragacanth were obtained after crosslinking with glutaraldehyde. New acetal bonds and simultaneous demethoxylation that form new free carboxylate groups after the GLU reaction were responsible for less packed biopolymeric structures. Thermal properties were improved after crosslinking. Such characteristics of crosslinked samples resulted in gels with layered morphology, higher water uptake ability and slightly enhanced mechanical properties. In addition, chemical and microstructural changes affect the MB adsorption process, resulting in hydrogels with improved adsorptive properties. The maximum absorption concentration of MB was q_m=530 mg/g of hydrogel. The adsorption could be well described by pseudo-second-order kinetic model and Langmuir isotherm model. TG GLU hydrogels are promising natural materials with diverse microstructures and properties, despite their complex structure. These properties give the hydrogels some features that make them suitable for practical applications related to the pharmaceutical industry for drug delivery, tissue engineering, and water remediation.

Acknowledgments

This work was supported by grants PROICO 2-2420 Universidad Nacional de San Luis and PIP-No559 CONICET.

Author Contribution

These authors contributed equally to work and all authors reviewed the manuscript.

Conflict of Interest

The authors declare no competing interests.

References

1. Qi X, Wu L, Su T, Zhang J, Dong W. Polysaccharide-based cationic hydrogels for dye adsorption. Colloids Surfaces B Biointerfaces. 2018;170:364–72.
2. Taghavizadeh Yazdi ME, Nazarnezhad S, Mousavi SH, Sadegh Amiri M, Darroudi M, Baino F, et al. Gum tragacanth (Gt): A versatile biocompatible material beyond borders. Molecules. 2021;26(6):1510.
3. Froelich A, Jakubowska E, Jadach B, Gadziński P, Osmałek T. Natural Gums in Drug-Loaded Micro-and Nanogels. Pharmaceutics. 2023;15(3):759.
4. Tanwar M, Gupta RK, Rani A. Natural gums and their derivatives based hydrogels: in biomedical, environment, agriculture, and food industry. Crit Rev Biotechnol. 2023;1–27.
5. Sudhakar K, Suneetha M, Rao KM, Han SS. Antibacterial reduced graphene oxide reinforces polyelectrolyte hydrogels with polysaccharides via a green method. Colloids Surfaces A Physicochem Eng Asp. 2021;628:127340.
6. Balaghi S, Mohammadifar MA, Zargaraan A, Gavlighi HA, Mohammadi M. Compositional analysis and rheological characterization of gum tragacanth exudates from six species of iranian astragalus. Food Hydrocoll. 2011;25(7):1775–84.
7. Boamah PO, Afoakwah NA, Onumah J, Osei ED, Mahunu GK. Physicochemical Properties, Biological Properties and Applications of Gum Tragacanth-A Review. Carbohydr Polym Technol Appl. 2023;100288.
8. Kiani A, Asempour H. Hydrogel membranes based on gum tragacanth with tunable structures and properties. II. Comprehensive characterization of the swelling behavior. J Appl Polym Sci. 2012;126(SUPPL. 1):E478–85.
9. Anderson DMW, Bridgeman MME. The composition of the proteinaceous polysaccharides exuded by astragalus microcephalus, a. gummifer and a. kurdicus. The sources of turkish gum tragacanth. Phytochemistry. 1985;24(10):2301–4.
10. Fattahi A, Petrini P, Munarin F, Shokoohinia Y, Golozar MA, Varshosaz J, et al. Polysaccharides derived from tragacanth as biocompatible polymers and gels. J Appl Polym Sci. 2013;129(4):2092–102.

11. Gavlighi HA, Meyer AS, Zaidel DNA, Mohammadifar MA, Mikkelsen JD. Stabilization of emulsions by gum tragacanth (astragalus spp.) correlates to the galacturonic acid content and methoxylation degree of the gum. Food Hydrocoll. 2013;31(1):5–14.

12. Bachra Y, Grouli A, Damiri F, Talbi M, Berrada M. A novel superabsorbent polymer from crosslinked carboxymethyl tragacanth gum with glutaraldehyde: Synthesis, characterization, and swelling properties. Int J Biomater. 2021;2021.

13. Gholamkhasi P, Kiani A. Swelling behavior of chitosan/tragacanth gum composite films crosslinked with glutaraldehyde. 2014;

14. Yang W, Qi G, Kenny JM, Puglia D, Ma P. Effect of cellulose nanocrystals and lignin nanoparticles on mechanical, antioxidant and water vapour barrier properties of glutaraldehyde crosslinked PVA films. Polymers (Basel). 2020;12(6):1364.

15. Mi FL, Kuan CY, Shyu SS, Lee ST, Chang SF. Study of gelation kinetics and chain-relaxation properties of glutaraldehyde-cross-linked chitosan gel and their effects on microspheres preparation and drug release. Carbohydr Polym. 2000;41(4):389–96.

16. Rahimdokht M, Pajootan E, Ranjbar-Mohammadi M. Titania/gum tragacanth nanohydrogel for methylene blue dye removal from textile wastewater using response surface methodology. Polym Int. 2019;68(1):134–40.

17. Aşık M, Akbay İK, Özdemir S, Genç R. pH-responsive self-healing of chemically modified tragacanth gum hydrogels as antibiotic release system. Int J Polym Mater Polym Biomater. 2021;1–11.

18. Ferdous A, Janta RA, Arpa RN, Afroze M, Khan M, Moniruzzaman M. The leaves of Bougainvillea spectabilis suppressed inflammation and nociception in vivo through the modulation of glutamatergic, cGMP, and ATP-sensitive K+ channel pathways. J Ethnopharmacol. 2020;261:113148.

19. Ghahestani SM, Shahab E, Karimi S, Madani MH. Methylene blue may have a role in the treatment of COVID-19. Med Hypotheses. 2020;144:110163.

20. Gamboni JE, Bertuzzi MA, Slavutsky AM. Methylene Blue Sorption Phenomena onto Pectin, Brea Gum, Montmorillonite Based Hydrogels: Kinetic and Thermodynamic Assessment. J Polym Environ. 2022;30(11):4710–25.

21. Mallakpour S, Tabesh F. Effective adsorption of methylene blue dye from water solution using renewable natural hydrogel bionanocomposite based on tragacanth gum: Linear-nonlinear calculations. Int J Biol Macromol. 2021;187:319–24.

22. Abbasi A, Khatoon F, Ikram S. A review on remediation of dye adulterated system by ecologically innocuous "biopolymers/natural gums-based composites." Int J Biol Macromol. 2023;123240.

23. Mallakpour S, Tabesh F. Green and plant-based adsorbent from tragacanth gum and carboxyl-functionalized carbon nanotube hydrogel bionanocomposite for the super removal of methylene blue dye. Int J Biol Macromol. 2021;166:722–9.

24. Jiang M, Simayi R, Sawut A, Wang J, Wu T, Gong X. Modified β-Cyclodextrin hydrogel for selective adsorption and desorption for cationic dyes. Colloids

Surfaces A Physicochem Eng Asp. 2023;130912.

25. Megbenu HK, Tauanov Z, Daulbayev C, Poulopoulos SG, Baimenov A. Effective removal of methylene blue dye by a novel 4-vinylpyridine-co-methacrylic acid cryogel: kinetic, isotherm, and breakthrough studies. J Chem Technol Biotechnol. 2022;97(12):3375–84.

26. Masuelli MA, Takara A, Acosta A. Hydrodynamic properties of tragacanthin. Study of temperature influence. J Argentine Chem Soc. 2013;100:25–34.

27. Cabello SDP, Takara EA, Marchese J, Ochoa NA. Influence of plasticizers in pectin films: Microstructural changes. Mater Chem Phys. 2015;162:491–7.

28. ASTM. ASTM D882-91: Standard test methods for tensile properties of thin plastic sheeting [Internet]. a. Vol. 87, Annual book of ASTM. Philadelphia, PA, USA; 1991. 95 p. Available from: www.astm.org

29. ASTM. ASTM E96 -E96M: Standard test methods for water vapor transmission of materials. b. Philadelphia, PA, USA; 2010. 12 p.

30. Nejatian M, Abbasi S, Azarikia F. Gum tragacanth: structure, characteristics and applications in foods. Int J Biol Macromol. 2020;160:846–60.

31. Lv H, Cui S, Zhang H, Pei X, Gao Z, Hu J, et al. Crosslinked starch nanofibers with high mechanical strength and excellent water resistance for biomedical applications. Biomed Mater. 2020;15(2):25007.

32. Silverstein RM, Webster FX, Kiemle D. Spectrometric Identification of Organic Compounds, 7th Edition [Internet]. Wiley; 2005. Available from: https://books.google.com.ar/books?id=mQ8cAAAAQBAJ

33. Fellah A, Anjukandi P, Waterland MR, Williams MAK. Determining the degree of methylesterification of pectin by ATR/FT-IR: Methodology optimisation and comparison with theoretical calculations. Carbohydr Polym. 2009;78(4):847–53.

34. Shi H, Wang Y, Hua R. Erratum: Acid-catalyzed carboxylic acid esterification and ester hydrolysis mechanism: Acylium ion as a sharing active intermediate via a spontaneous trimolecular reaction based on density functional theory calculation and supported by electrospray ioniza. Phys Chem Chem Phys. 2015;17(48):32571–3.

35. Saruchi, Kaith BS, Jindal R, Kapur GS. Synthesis of gum tragacanth and acrylic acid based hydrogel: its evaluation for controlled release of antiulcerative drug pantoprazole sodium. J Chinese Adv Mater Soc. 2014;2(2):110–7.

36. Jenova I, Venkatesh K, Karthikeyan S, Madeswaran S. Characterization of proton conducting polymer blend electrolyte based on gum tragacanth and polyvinyl alcohol. Mater Today Proc. 2023;

37. Mohammadian M, Sahraei R, Ghaemy M. Synthesis and fabrication of antibacterial hydrogel beads based on modified-gum tragacanth/poly (vinyl alcohol)/Ag0 highly efficient sorbent for hard water softening. Chemosphere. 2019;225:259–69.

38. Alba K, Bingham RJ, Gunning PA, Wilde PJ, Kontogiorgos V. Pectin conformation in solution. J Phys Chem B. 2018;122(29):7286–94.

39. Zohuriaan MJ, Shokrolahi F. Thermal studies on natural and modified gums. Polym Test. 2004;23(5):575–9.

40. Shirzadian T, Nourbakhsh MS, Fattahi A, Bahrami G, Mohammadi G. Characterization and optimization of de-esterified tragacanth-chitosan nanocomposite as a potential carrier for oral delivery of insulin: In vitro and ex vivo studies. J Biomed Mater Res - Part A. 2021;109(11):2164–72.

41. Sadrjavadi K, Shahbazi B, Fattahi A. De-esterified tragacanth-chitosan nano-hydrogel for methotrexate delivery; optimization of the formulation by taguchi design. Artif Cells, Nanomedicine Biotechnol. 2018;46(sup2):883–93.

42. Einhorn-Stoll U, Kastner H, Fatouros A, Krähmer A, Kroh LW, Drusch S. Thermal degradation of citrus pectin in low-moisture environment – investigation of backbone depolymerisation. Food Hydrocoll. 2020;107:105937.

43. Fatouros A, Einhorn-Stoll U, Kastner H, Drusch S, Kroh LW. Influence of the carboxylic function on the degradation of d -galacturonic acid and its polymers. J Agric Food Chem. 2021;69(32):9376–82.

44. Yildirim M, Hettiarachchy NS. Biopolymers produced by cross-linking soybean 11S globulin with whey proteins using transglutaminase. J Food Sci. 1997;62(2):270–5.

45. Reddy N, Reddy R, Jiang Q. Crosslinking biopolymers for biomedical applications. Trends Biotechnol. 2015;33(6):362–9.

46. Pasini Cabello SD, Ochoa NA, Takara EA, Mollá S, Compañ V. Influence of pectin as a green polymer electrolyte on the transport properties of chitosan-pectin membranes. Carbohydr Polym. 2017;157:1759–68.

47. Einhorn-Stoll U, Kastner H, Urbisch A, Kroh LW, Drusch S. Thermal degradation of citrus pectin in low-moisture environment. Influence of acidic and alkaline pre-treatment. Food Hydrocoll. 2019;86:104–15.

48. Singh B, Sharma V. Crosslinking of poly(vinylpyrrolidone)/acrylic acid with tragacanth gum for hydrogels formation for use in drug delivery applications. Carbohydr Polym. 2017;157:185–95.

49. Jridi M, Bardaa S, Moalla D, Rebaii T, Souissi N, Sahnoun Z, et al. Microstructure, rheological and wound healing properties of collagen-based gel from cuttlefish skin. Int J Biol Macromol. 2015;77:369–74.

50. Rana V, Rai P, Tiwary AK, Singh RS, Kennedy JF, Knill CJ. Modified gums: Approaches and applications in drug delivery. Carbohydr Polym. 2011;83(3):1031–47.

51. Singh B, Sharma V. Influence of polymer network parameters of tragacanth gum-based pH responsive hydrogels on drug delivery. Carbohydr Polym. 2014;101(1):928–40.

52. Kirtil E, Aydogdu A, Svitova T, Radke CJ. Assessment of the performance of several novel approaches to improve physical properties of guar gum based biopolymer films. Food Packag Shelf Life. 2021;29:100687.

53. Acevedo-Fani A, Salvia-Trujillo L, Rojas-Graü MA, Martín-Belloso O. Edible

films from essential-oil-loaded nanoemulsions: Physicochemical characterization and antimicrobial properties. Food Hydrocoll. 2015;47:168–77.

54. Saurabh CK, Gupta S, Bahadur J, Mazumder S, Variyar PS, Sharma A. Mechanical and barrier properties of guar gum based nano-composite films. Carbohydr Polym. 2015;124:77–84.